Supplementary Information

Observation of Road Salt Aerosol Driving Inland Wintertime Atmospheric Chlorine Chemistry

Stephen M. McNamara[1], Katheryn R. Kolesar[1,a], Siyuan Wang[1,b], Rachel M. Kirpes[1], Nathaniel W. May[1], Matthew J. Gunsch[1], Ryan D. Cook[1], Jose D. Fuentes[2], Rebecca S. Hornbrook[3], Eric C. Apel[3], Swarup China[4], Alexander Laskin[4,c], Kerri A. Pratt[1,5*]

[1]Department of Chemistry, University of Michigan, Ann Arbor, MI, USA
[2]Department of Meteorology and Atmospheric Science, The Pennsylvania State University, University Park, PA, USA
[3]Atmospheric Chemistry Observations & Modeling Laboratory, National Center for Atmospheric Research, Boulder, CO, USA
[4]Environmental Molecular Sciences Laboratory, Pacific Northwest National Laboratory, Richland, WA, USA
[5]Department of Earth and Environmental Sciences, University of Michigan, Ann Arbor, MI USA
[a]Present address: Air Sciences Inc., Portland, OR, USA
[b]Present address: Atmospheric Chemistry Observations & Modeling, National Center for Atmospheric Research, Boulder, CO, USA
[c]Present address: Department of Chemistry, Purdue University, West Lafayette, IN, USA

*Corresponding Author: Kerri A. Pratt
Department of Chemistry
University of Michigan, Ann Arbor
930 N. University Ave.
Ann Arbor, MI 48109 USA
prattka@umich.edu
(734) 763-2871

Table of Contents:

SECTION S1. ADDITIONAL METHODS

S1.1 Chemical ionization mass spectrometry (CIMS)

Here, we briefly describe the post-campaign calibration procedures for HNO_3, $ClNO_2$, and N_2O_5. The HNO_3 calibration was completed using a 50 ng min^{-1} HNO_3 permeation source (VICI Metronics, Inc.), the permeation rate of which was confirmed by impinging the HNO_3 in N_2 into 4 mL of nanopure H_2O for 40 min. The resulting nitrate concentration was analyzed using ion chromatography. Following the method of *Thaler et al.,*[1] $ClNO_2$ was synthesized by passing Cl_2 over 1 mL of 0.1 M $NO_2^-{}_{(aq)}$ solution in a Pyrex reaction vessel. The $ClNO_2$ was then passed through a 300°C quartz tube oven to induce thermal dissociation, generating Cl and NO_2. Generated NO_2 (0.1 – 1 ppb range) was directly related to the amount of thermally-dissociated $ClNO_2$ and quantified using a NO chemiluminescence detector (THS Instruments)[2] equipped with a photolytic NO_2 to NO converter.[3] N_2O_5 was synthesized by reacting NO_2 with ppb levels of O_3 in a PFA Teflon tube, similar to *Bertram et al*.[4] The N_2O_5 was quantified (0.1 – 1.5 ppb range) by monitoring the change in NO_2, measured by the NO chemiluminescence detector[2] following

photolytic conversion of NO_2.[3] It was assumed that two moles of NO_2 were consumed for every 1 mole of N_2O_5 produced. Since the quantification of N_2O_5 depends on the complete conversion of NO_2 to N_2O_5, it is important that no other species (e.g. $ClNO_2$, HNO_3) were generated as byproducts during this process. During calibration for N_2O_5, minimal amounts of $ClNO_2$ (average 0.40 ± 0.06% of total N_2O_5) were formed, with no HNO_3 observed. Additionally, given the conditions within the PFA reaction vessel ([NO_2] at ~40 ppb), the contribution from NO_3 was calculated to be negligible (only 4% of [N_2O_5]). Therefore, the assumption that $\Delta[NO_2]/2 = \Delta[N_2O_5]$ is reasonable. The calibration factors, relative to Cl_2 (at *m/z* 197), were measured to be 3.7 ± 0.4, 0.84 ± 0.08, and 2.3 ± 0.5 for $ClNO_2$, N_2O_5, and HNO_3, respectively.

The CIMS sampling line was tested post-campaign for off-gassing of $ClNO_2$, N_2O_5 and HNO_3 to rule out sampling artifacts. The sampling line was purged with dry N_2; $ClNO_2$, N_2O_5, and HNO_3 signals remained below limits of detection. N_2O_5 was introduced into the sampling line, post campaign, to determine if $ClNO_2$ would be generated as an artifact. Similar to previous studies,[5] when 400 – 500 ppt N_2O_5 was introduced into the sampling line, only 0.6 ± 0.4% of the N_2O_5 was converted to $ClNO_2$. The same test was performed with Cl_2; the addition of 6 – 18 ppb of Cl_2 into the sampling resulted in the formation of only ~1 ppt $ClNO_2$. However, during the ambient measurements, Cl_2 was not observed above the 2 ppt CIMS detection limit, suggesting that this mechanism did not contribute to the observed $ClNO_2$. In addition, during the ambient measurements, there were multiple observations of N_2O_5 in the absence of, or in the presence of very little $ClNO_2$, such as February 4 and the early evening of February 29 (**Figure S1**), further confirming the lack of sampling line artifacts during the campaign.

S1.2 Ambient ion monitor - ion chromatograph (AIM-IC)

Online $PM_{2.5}$ Cl^-, NH_4^+, NO_3^-, and SO_4^{2-}, and gas-phase NH_3, HCl, and SO_2 measurements were performed using an ambient ion monitor-ion chromatography (AIM-IC) system, described in detail by *Markovic et al.,*[6] from February 3 to March 10, 2016 using 1 h sampling resolution. Briefly, the AIM-IC consists of two main components: (i) the sample collection unit – where water soluble gases and $PM_{2.5}$ are collected into aqueous solutions (AIM 9000D, URG Corp.), and (ii) the sample analysis unit – where anions and cations are analyzed by ion chromatography (Dionex ICS-2100 and ICS-1100, respectively, Thermo Scientific). The 3σ LODs for $HCl_{(g)}$, $SO_{2(g)}$, $NH_{3(g)}$, $Cl^-_{(p)}$, $NO_3^-{}_{(p)}$, $SO_4^{2-}{}_{(p)}$, and $NH_4^+{}_{(p)}$ were 90 ppt, 8 ppt, 70 ppt, 0.04 μg m^{-3}, 0.01 μg m^{-3}, 0.02 μg m^{-3}, and 0.06 μg m^{-3}, respectively. The ion chromatographs were calibrated offline by injecting mixed standards of anions (P/N 56933, Thermo Scientific) and cations (P/N 40187, Thermo Scientific) directly into the corresponding concentrators through the injection valves. Additionally, standard samples of road salts and brines used by the city of Ann Arbor and UM were obtained for offline chemical analysis by IC, as well as atomized salt/brine by ATOFMS (**Section S2.4**).

Sample collection began by drawing ambient air at 3 L min^{-1} through a 1.3 m long insulated sampling inlet to a size-selection assembly with a 2.5 μm cut inertial impactor. Next, the ambient air flowed through the parallel-plate wet denuder (PPWD), made of two nylon membranes that were constantly supplied with a 5.5 mM $H_2O_{2(aq)}$ solution at 10 mL h^{-1}. In the PPWD, soluble gases (HCl, SO_2, NH_3) diffused and dissolved into the denuder solution. The air flow continued into the particle supersaturation chamber (PSSC), where particles were collected in solution by inertial impaction. The PSSC consists of a steam generator, water condensation chamber, and cyclone that activate, grow, and remove particles from the air stream. The PPWD and PSSC solution outflows containing dissolved gases and $PM_{2.5}$, respectively, were each split in two, and each solution was collected into a separate 5 mL syringe through a 6-port injection valve (Rheodyne LLC, Rohnert

Park, CA). The collected samples in four separate syringes were injected by the syringe pump into four separate ion concentrators at the end of the 1 h sampling period, and the sample collection with the syringe pump restarted at the top of the hour. The two fractions of the aqueous particle sample were analyzed for anion and cation composition at the top of the hour. The two fractions of the collected aqueous gas sample fractions are then analyzed during the second half of the hour.

The ICS-1100 (cation) and ICS-2100 (anion) ion chromatographs used to analyze water-soluble $PM_{2.5}$ and gases were equipped with ultralow pressure trace concentrator columns for reagent-free IC (ICS-1100: TCC-ULP1, 5 x 23 mm, Thermo Scientific; ICS-2100: UTAC-ULP1, 5 x 23 mm, Thermo Scientific). The ICS-1100 and ICS-2100 were each equipped with a guard column (ICS-1100: IonPac CG12A-5 µm, 3 x 30 mm, Thermo Scientific; ICS-2100: IonPac AG18, 4 x 50 mm, Thermo Scientific), analytical column (ICS-1100: IonPac CS12A-5 µm, 3 x 150 mm, Thermo Scientific; ICS-2100: IonPac AS18 4 mm Analytical Column, 4 x 250 mm, Thermo Scientific), suppressor (ICS-1100: Dionex CSRS 500, 4 mm, Thermo Scientific: ICS-2100: Dionex AERS500, 4 mm, Thermo Scientific), and conductivity detector (Dionex DS6 Heated Conductivity Cell, Thermo Scientific). Methanesulfonic acid (20 mM) was used as the eluent for the cation column and a KOH gradient, generated by an EGC III KOH system (Thermo Scientific), was used as the eluent for the anion column.

S1.3 Nitric oxide (NO) and volatile organic compounds (VOCs)

Atmospheric nitric oxide (NO) was measured from February 11 – March 9, 2016 using a chemiluminescence detector[2] with a flow rate of 0.96 L min^{-1} through a 4 m long, 0.16 cm ID PFA insulated inlet. Humidified N_2 was added to the ambient flow at 0.12 L min^{-1} to ensure a constant, low, background signal. Background measurements were taken for 80 s every 20 min. Multi-point calibration of the NO chemiluminescence detector, using NO mole ratios ranging from 0 to 25 ppb,

was performed post-campaign using a 1.1 ± 0.1 ppm NO (in N_2) standard cylinder (Metro Welding Supply Corp., Detroit, MI).

Stainless steel canisters were used for whole air sampling and offline analysis of volatile organic compounds. The canisters were cleaned and evacuated prior to sampling. During sampling, the canisters were pressurized for ~1 h at 101-103 mL min^{-1}. The canisters were analyzed using the Trace Organic Gas Analyzer (TOGA)[7] for HCHO and CH_3CHO, and a gas chromatograph with a flame-ionization detector (GC-FID) for C_2-C_4 alkanes.[8,9] The GC-FID was calibrated using a National Institute of Standards and Technology (NIST) prepared mixture of alkanes in N_2 using a dynamic dilution system. The FID analysis uncertainty is estimated to be within ± 5%. The TOGA was calibrated for HCHO and CH_3CHO using in-house ppb-level standards using the same dynamic dilution system,[10] with estimated uncertainties for HCHO and CH_3CHO of ± 30%, largely due to uncertainties in their stability in canisters.

S1.4 Aerosol size distribution measurements

A scanning mobility particle sizer spectrometer (SMPS, model 3082, TSI Inc.) and aerodynamic particle sizer (APS, model 3321, TSI Inc.) measured aerosol size distributions and surface area concentrations during the campaign. The shared inlet consisted of a 122 cm long, 1.72 cm ID unheated, insulated copper tube connected to a stainless-steel sampling manifold, with insulated sampling lines for each instrument, as well as the aerosol time of flight mass spectrometer (**Section 4.2.1**). The total flow rate through the inlet and sampling manifold was 10 L min^{-1}. The SMPS consisted of a model 3081 differential mobility analyzer (DMA, TSI Inc.) and a model 3775 condensation particle counter (CPC, TSI Inc.) and sampled through a 0.48 cm ID copper sampling line. The SMPS was operated with a sheath flow rate of 2.5 L min^{-1} and an aerosol flow rate of 0.3 L min^{-1} to measure particles from 15 – 850 nm (mobility diameter, d_m). The APS sampled air at 5

L min^{-1} through a 0.79 cm ID copper sampling line. The APS measured size-resolved particle number concentrations from 0.54 – 20 μm (aerodynamic diameter, d_a).

S1.5 Conversion of projected area diameter to aerodynamic diameter

Single particle projected area diameter (d_{pa}), measured by CCSEM-EDX, is based on the measured diameter of a non-spherical particle impacted on the substrate. In order to use the CCSEM-EDX particle diameter to calculate chemically-resolved surface area concentrations using the merged aerosol size distribution data (in aerodynamic diameter, d_a, **Methods**), the d_{pa} for each particle was converted to d_a (assumed to be spherical) based on the methods of *Wagner & Leith*:[11]

$$d_a = \frac{d_{pa}}{S_v * \sqrt{\frac{\rho_p}{S_D * \rho_0}}} \quad \text{SE1}$$

$$S_V = \frac{1}{C_p,i} \quad \text{SE2}$$

where S_V is the volumetric shape factor, determined for each particle type identified in **Section 4.3** of the **Methods**, based on CCSEM-EDX particle circularity (c_p,i) using Equation SE2.[11] S_D is the aerodynamic shape factor (aerodynamic diameters are assumed to be spherical, so S_D = 1). ρ_p is the particle density, dependent on particle class ($\rho_{road\ dust}$ = 2.0 g cm^{-3}, $\rho_{road\ salt}$ = 1.5 g cm^{-3}, $\rho_{biomass\ burning}$ = 1.4 g cm^{-3}, $\rho_{aged\ road\ salt}$ = 1.45 g cm^{-3}, and ρ_{soot} = 1.4 g cm^{-3}) [12], and ρ_0 is the unit density (1 g cm^{-3}).

S1.6 Turbulent transport in the 1-D model

The turbulent diffusivity K is given as:[13]

$$K = \frac{\kappa z u^* \left(1 - \frac{z}{Z_{ABL}}\right)^{1.5}}{\phi_H(\xi)} \quad \text{SE3}$$

where κ is the von Karman constant (=0.4), u_* is the friction velocity (m s^{-1}), Z_{abl} is the atmospheric boundary layer height (m), φ_H is the stability correct function for heat, and ζ is a dimensionless term defined as the ratio of z/L (L: Obukhov length scale, in m).

$$u^* = \frac{\kappa U_{ref}}{ln\left(\frac{z_{ref}-d}{z_0}\right)-\Psi_m(\xi)} \quad \text{SE4}$$

U_{ref} is the horizontal wind speed (m s^{-1}) measured at the reference height of 12 m (z_{ref}), d is the displacement length (7.2 m, ~60% of reference height),[13] z_0 is the aerodynamic roughness length (m), which was chosen as 0.5 m, corresponding to a small city center,[13] and Ψ_m is the integrated form of stability correction function for momentum.

Model boundary layer conditions are derived based on sounding data provided by the University of Wyoming (http://weather.uwyo.edu/upperair/sounding.html) obtained on February 17-18 and March 7-8, 2016 at 7:00 and 19:00 EST at the Detroit Metropolitan Airport (42.2194°N, 83.3705°W), ~30 km to the east of Ann Arbor. Due to the lack of high time resolution soundings, the boundary layer structure and stability were interpolated between the morning sounding collected at 07:00, indicative of the boundary layer of the previous night, and the evening sounding collected at 19:00, representative of the daytime boundary layer. The vertical profiles of horizontal wind speed (U) and potential temperature (θ) are used to calculate the Obukhov length scale, L:[14]

$$L \cong \frac{u^*\theta}{\kappa g}\frac{\Delta U}{\Delta \theta} \quad \text{SE5}$$

SECTION S2. RESULTS AND DISCUSSION

S2.1 Atmospheric trace gas and particle observations

The full time series of $ClNO_2$ and N_2O_5 CIMS measurements, from February 1 to March 10, is shown in **Figure S1**. Hourly average mole ratios of HNO_3 and HCl are shown in **Figure S4**. Of particular interest to the multiphase production of $ClNO_2$ is $PM_{2.5}$ containing chloride and nitrate (**Figure S4**). The average concentration of $PM_{2.5}$ chloride was 0.062 ± 0.003 μg m^{-3} (95% CI) from February 8 to March 10, 2016. Data are not available for $PM_{2.5}$ chloride from February

3-8, 2016 due to an instrument background issue that was subsequently fixed. The average concentration of $PM_{2.5}$ nitrate was 2.4 ± 0.2 μg m^{-3} (95% CI) during the field campaign.

The two case periods experienced different levels of $ClNO_2$ (measured maxima of 98 ppt during February 17-18 versus 22 ppt during March 7-8, **Figure 3**), likely due to higher N_2O_5 during February 17-18 (average of 227 ppt) in comparison to March 7-8, when N_2O_5 was 59% lower (average of 92 ppt). However, despite a larger average aerosol surface area concentration (**Figure S5**) during March 7-8 (229 μm^2 cm^{-3}) than during February 17-18 (174 μm^2 cm^{-3}), the contribution of road salt aerosol was lower in March (**Figure 2**). The time-resolved particle size distributions for the two case study time periods are shown in **Figure S5**, from which total particle surface area concentrations were subsequently calculated during these periods. **Table S2** contains the average mole ratios for specific volatile organic compounds collected on February 10 and 12, 2016. The average of two samples (10:15 – 11:26 February 10, 2016 and 10:58 – 12:30 February 12, 2016) is used for model simulations of the case study days.

S2.2 October measurements of $ClNO_2$

CIMS measurements were also made at the same location on the University of Michigan campus from October 23-28, 2016 (**Figure S6**). There was no road salt applied on the Ann Arbor, MI roads in October 2016. The first snowfall in Ann Arbor for winter 2016-2017, approximately corresponding to the first road salting, was on November 20, 2016. While nightly formation of N_2O_5 was observed, the nightly increase in $ClNO_2$ was much less pronounced. Average nightly $ClNO_2$ was approximately seven times lower in October (3.5 ± 0.5 ppt, 95% CI), compared to February – March 2016 (23 ± 1 ppt, **Figure S1**). The average nightly N_2O_5 was a factor of two lower in October (71 ± 5 ppt), as compared to February to March 2016 (141 ± 7 ppt), likely due to higher temperatures in October 2016 (range of -3° to 19°C, average 6°C), compared to February

to March 2016 (range of -19 to 20°C, average 0°C). Temperatures during the October 2016 period were higher than the February 17-18 case period (range of -12° to -1°C, average -6°C), but similar to the March 7-8 case period (range of 10° to 18°C, average 12°C). The October 2016 maxima for $ClNO_2$ (29 ppt) and N_2O_5 (698 ppt) were both lower than the February to March 2016 maxima (220 ppt $ClNO_2$ and 2466 ppt N_2O_5). These results are consistent with previous fall $ClNO_2$ measurements in Calgary, Alberta that showed a maximum of 30 ppt during September 2010, before the first snowfall, compared to a maximum of 338 ppt during March 2011.[15]

S2.3 Chemical composition of road salt used in Ann Arbor, MI

Standard samples of road salts and brines used by the city of Ann Arbor, MI and the University of Michigan (UM) were obtained for chemical analysis by IC. Both the city of Ann Arbor and UM used a brine solution and road salt during deicing. Additionally, UM used brine to spray sidewalks. Sodium was the dominant cation in the UM brine, UM road salt, and Ann Arbor road salt, while calcium was the dominant cation in Ann Arbor brine (**Figure S7**). Chloride was the dominant anion measured in all samples, confirming the presence of chloride salts; SO_4^{2-}, NO_3^-, NO_2^-, PO_4^{3-}, and Br^- were all below the IC detection limits. The UM and Ann Arbor road salt samples and the UM brine samples were primarily composed of NaCl, with measured Cl^-/Na^+ mole ratios of 0.96 ± 0.05, 1.00 ± 0.02, and 0.97 ± 0.01, respectively. UM and Ann Arbor road salt samples were also dissolved in nanopure water and aerosolized with an atomizer into the ATOFMS for individual particle analysis. Average individual particle ATOFMS mass spectra of aerosolized road salt are shown in **Figure S7**.

S2.4 Consideration of potential other chloride sources

S2.4.1 Transported power plant/industrial plumes

Gas-phase HCl and molecular chlorine, Cl_2, are additional potential sources of chlorine in urban areas.[16–18] Both $ClNO_2$ and Cl_2 photolyze to produce Cl radicals, which react with volatile organic compounds to form HCl.[19] HCl gas can also be directly emitted from power plants and industrial activity, and is regulated by the US Environmental Protection Agency.[20] In the current study, Cl_2 was never observed above its 2 ppt CIMS LOD. HCl was of minimal influence due to its low observed concentration, which was typically below the 90 ppt LOD (72% of measurements). Nevertheless, because this study aims to characterize local production of $ClNO_2$, we identified time periods potentially influenced by transported plumes from power plants and industrial activity[16] (**Figure S8**). Of the top-fifteen largest HCl-emitting facilities in the state of Michigan in 2016 (HCl emissions of 11,500 – 210,000 lbs yr^{-1}), five facilities are located in the Southeast Michigan region.[20] These facilities, three of which are fossil fuel power plants, are all located approximately 50 km to the east and southeast in the cities of River Rouge (three facilities), Trenton (one facility), and Monroe (one facility). In addition, smaller power plants and other industrial sites are located predominantly within the nearby metropolitan Detroit region. Therefore, we identified time periods when winds came from 15° to 150° (north-northeast to southeast with respect to the sampling site) as potentially influenced by power plants and industry; these air masses accounted for ~16% of the period between February 3 and March 10, 2016 (**Figure S8**). During these periods, SO_2 was often elevated (typically >1 ppb), compared to the non-plume periods (average of 0.24 ± 0.02 ppb). However, HCl did not follow the same trend, exhibiting similar average levels between plume (103 ± 6 ppt) and non-plume periods (126 ± 6 ppt) for times with data above the 90 ppt LOD, demonstrating that the sampling site was not significantly impacted by HCl emissions from the north-northeast to southeast.

During the February 17-18 case study day, the period from 07:00 to 12:00 (February 18) experienced winds from the east-southeast (90°-100°), consistent with the plume-influenced area (**Figure S8**). However, because HCl was not elevated above LOD, and this occurred after sunrise when $ClNO_2$ was being photolyzed (rather than produced), there likely was not significant influence from transported power plant/industrial plumes during this time. Additionally, during the night of the March 7-8 case period (22:00 – midnight), the winds briefly shifted from the south (~180°) to the southeast (130°-140°). However, wind speeds were <0.5 m s^{-1}, and HCl and SO_2 were not elevated during this two-hour period, again likely ruling out power plant/industrial plume influence.

S2.4.2 Other sources of chloride containing aerosol

Ammonium chloride (NH_4Cl) in the particle phase can exist in equilibrium with gas-phase HCl and ammonia.[21] Ammonium was primarily observed, by ATOFMS, within the biomass burning particles (**Figure S2**). As observed previously in wintertime Toronto,[22] ammonium was primarily present as ammonium nitrate and ammonium sulfate, since nearly all biomass burning particles contained nitrate and most contained sulfate; in comparison, few biomass burning particles contained chloride (8-18%, by number, on the February 17-18 and March 7-8 case days) (**Figure S2**), suggesting limited contribution from ammonium chloride. Previous work has observed higher NH_3, HCl, and HNO_3 concentrations than predicted based on thermodynamic equilibrium for temperatures <5°C or relative humidities below 80%,[23,24] which are relevant to the conditions of our study. The previous coastal $ClNO_2$ study by *Ryder et al.,*[25] that included single-particle mass spectrometry observations, discussed that HCl and HNO_3 are often not observed to be in equilibrium with the particle phase, especially for supermicron particles, in part due to inter-particle variability in pH, liquid water content, and organic films, which likely also impacted the

particle population in this study. Chloride can also be emitted as a component of fresh biomass burning particles and lead to $ClNO_2$ production;[26] therefore, we included $ClNO_2$ production from biomass burning particles in the model, as described in **Section 4.5.2**.

S2.5 Meteorology

Hourly average temperature, relative humidity, and wind speed and direction are shown in **Figure S9**. Data verification information for this weather station is available through the Citizen Weather Observer Program (CWOP, http://weather.gladstonefamily.net/site/d7729). Air temperature ranged from -18.5°C on February 14, 2016 at 07:39 EST to 20.3°C on March 9, 2016 at 12:39 EST. For the February 17-18 case period, winds were mainly from the north, with an average speed of 0.9 m s^{-1}, an average RH of 70% with a range of 54-87%, and an average air temperature of -6°C (minimum -12°C, maximum -1°C). For the March 7-8 case period, winds were mainly from the south, with an average speed of 1.4 m s^{-1}, an average RH of 70% with a range of 58-78%, and an average air temperature of 12°C (minimum 10°C, maximum 18°C). The selection of the two case study periods was primarily based on the relatively stable meteorological conditions observed during these two days.

SECTION S3. SUPPLEMENTARY FIGURES AND TABLES

Table S1 | γ_{N2O5} and φ_{ClNO2} values assigned for each single-particle type, expected to be deliquesced, as discussed in the Methods, with laboratory-based proxies and references provided.

Particle Type	γ_{N2O5}	φ_{ClNO2}	Particle types used as proxies for N_2O_5 uptake	References
Road Salt	0.03	1.0	NaCl	Behnke et al.,[27] Bertram and Thornton,[28] Chang et al.[29]
Aged Road Salt	0.01	0.2	Mixed $NaNO_3$ and NaCl	Behnke et al.,[27] Bertram and Thornton[28]
Biomass Burning	0.03	0.2	Malonic acid	Chang et al.[29]
Road Dust	0.013	0	Saharan dust	Crowley et al.[30]
Soot	2×10^{-4}	0	Graphite (from spark generator)	Saathoff et al.[31]

Table S2 | Average mole ratios of specific volatile organic compounds on February 10 and 12, 2016.

Species	Mole ratio (ppb)
C_2H_6	4.12
C_3H_8	1.49
n-C_4H_{10}	0.74
i-C_4H_{10}	0.31
HCHO	1.86
CH_3CHO	4.69

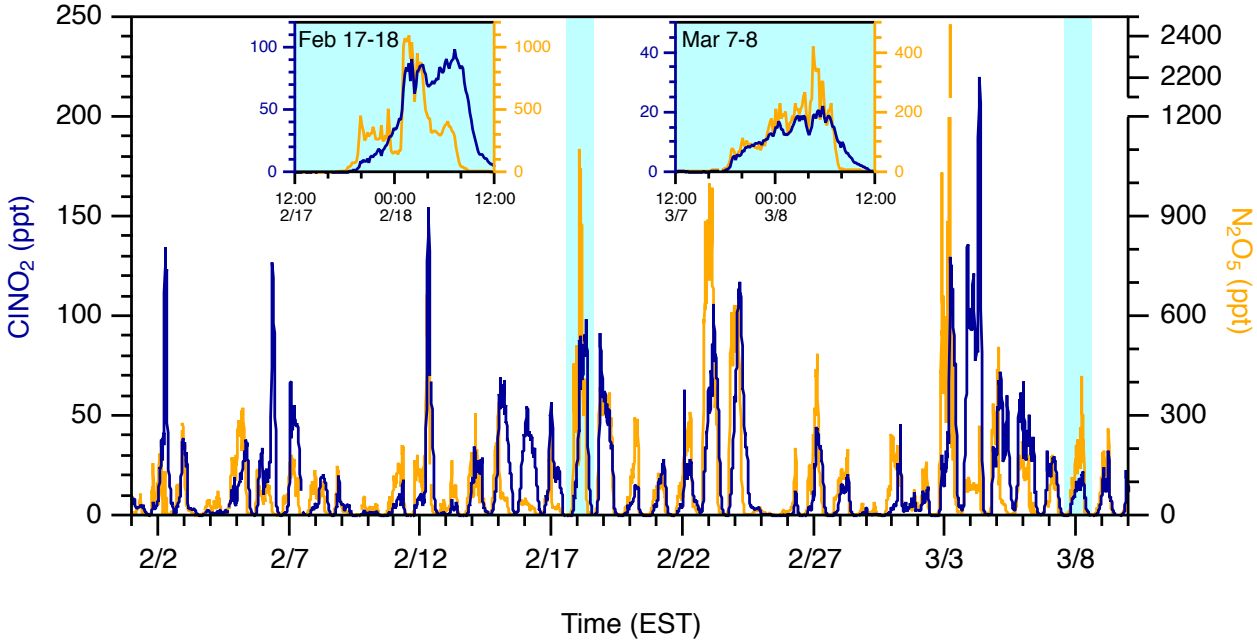

Figure S1 | Wintertime $ClNO_2$ and N_2O_5 observations in Ann Arbor, Michigan. 10 min averaged $ClNO_2$ and N_2O_5 mole ratios, measured by CIMS, from February 1 to March 10, 2016. The blue shaded regions represent two case periods (February 17-18 and March 7-8, 2016), with insets of those periods shown.

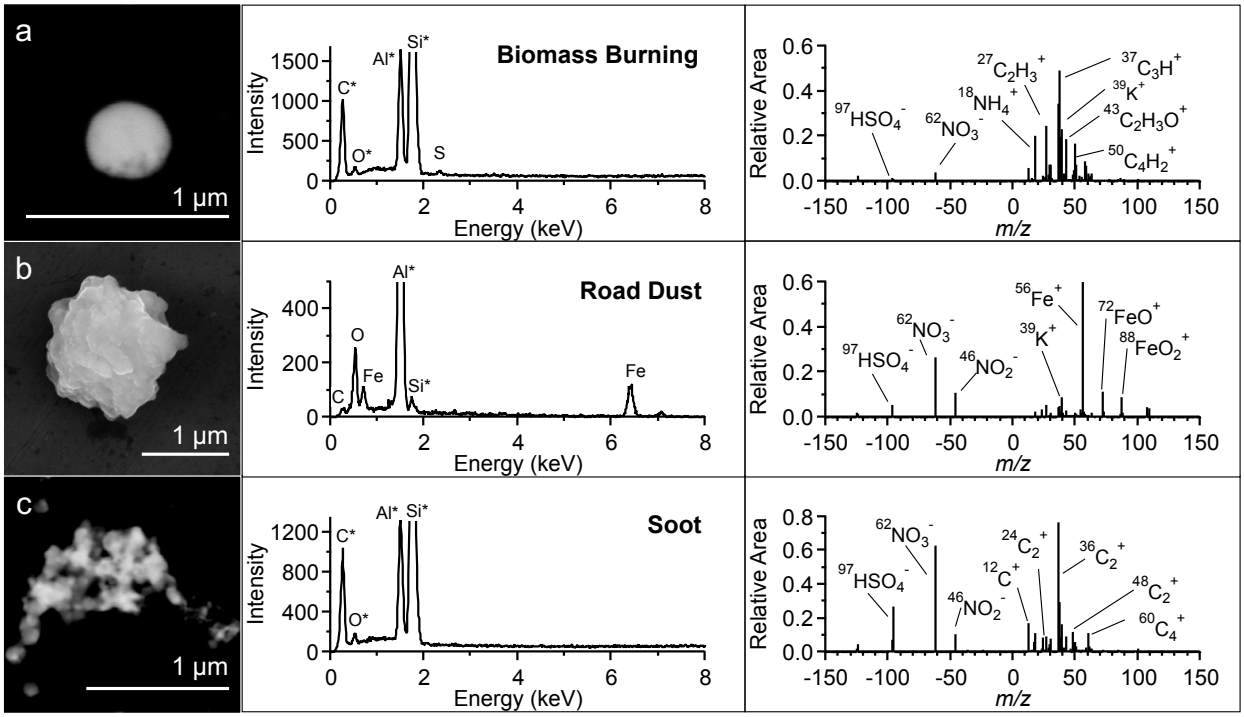

Figure S2 | Identification and quantitation of additional observed particle types. Representative SEM images (*left*) and EDX spectra (*middle*), and average ATOFMS dual-polarity mass spectra (*right*) for the three additional particle types observed during the study: (**a**) biomass burning, (**b**) road dust, and (**c**) soot. In the EDX spectra, the asterisks (*) indicate some signal from the substrate and/or detector backgrounds.

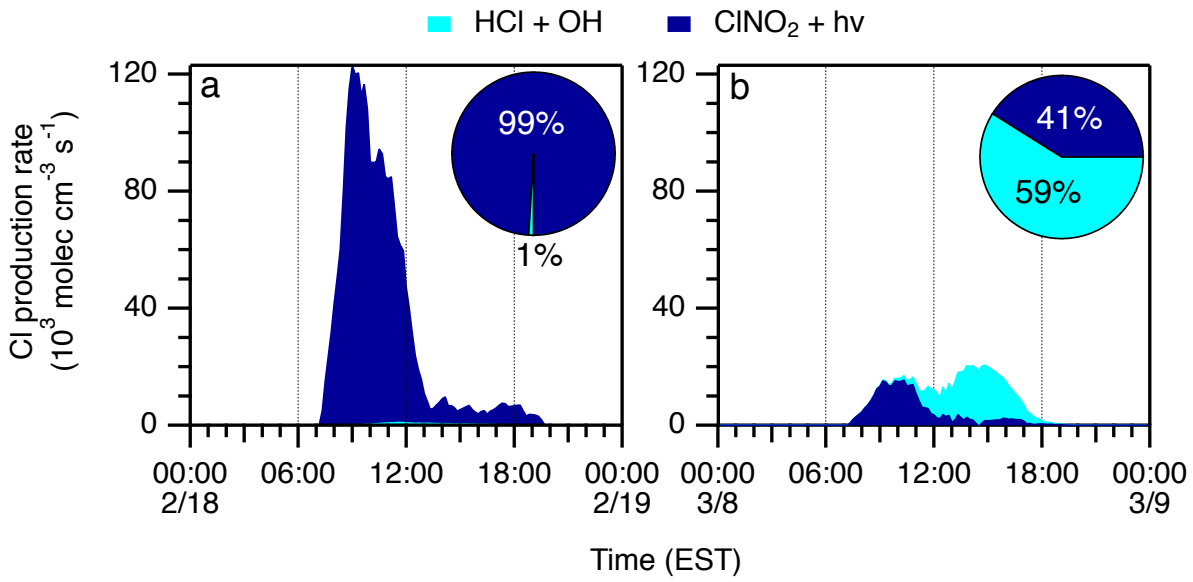

Figure S3 | Road salt-sourced $ClNO_2$ is a major contributor to chlorine atom production. Calculated chlorine (Cl) atom production rate via two pathways: HCl + OH and $ClNO_2$ photolysis. Used in the calculation are $ClNO_2$ and HCl measurements, modeled OH (maxima: (3.4 – 5.0) x 10^6 molecules cm^{-3}), and the $ClNO_2$ photolysis rate (j_{ClNO2}) calculated using the National Center for Atmospheric Research Tropospheric Ultraviolet and Visible (TUV) model (https://www2.acom.ucar.edu/modeling/tropospheric-ultraviolet-and-visible-tuv-radiation-model). Dates shown are the daytime periods following the modeled nighttime periods in Figure 3: (**a**) 00:00 February 18 to 0:00 February 19, and (**b**) 00:00 March 8 to 0:00 March 9.

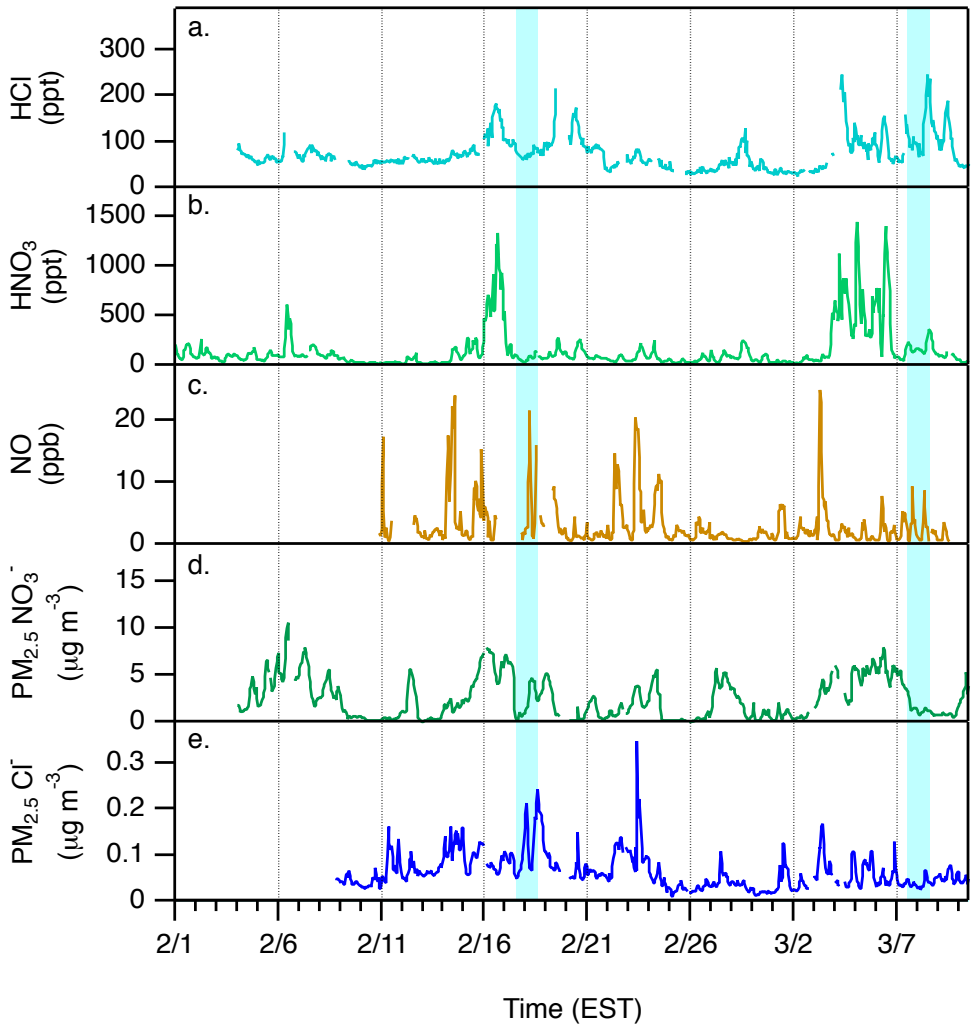

Figure S4 | Additional measurements of trace gas and particle species. (**a-c**) Hourly averaged mole ratios of (**a**) HCl (converted to ppt based on standard temperature and pressure, STP) from AIM-IC measurements, (**b**) HNO_3 from CIMS measurements, and (**c**) NO from the NO analyzer. (**d-e**) AIM-IC hourly averaged mass concentrations of $PM_{2.5}$ nitrate ($NO_3^-{}_{(p)}$, **d**) and chloride ($Cl^-{}_{(p)}$, **e**). AIM-IC measurements started on February 3 (except $PM_{2.5}$ Cl^-, which started on February 8), CIMS measurements started on February 1, and NO measurements started on February 11, 2016. The blue shaded regions represent the two case periods (February 17-18 and March 7-8, 2016).

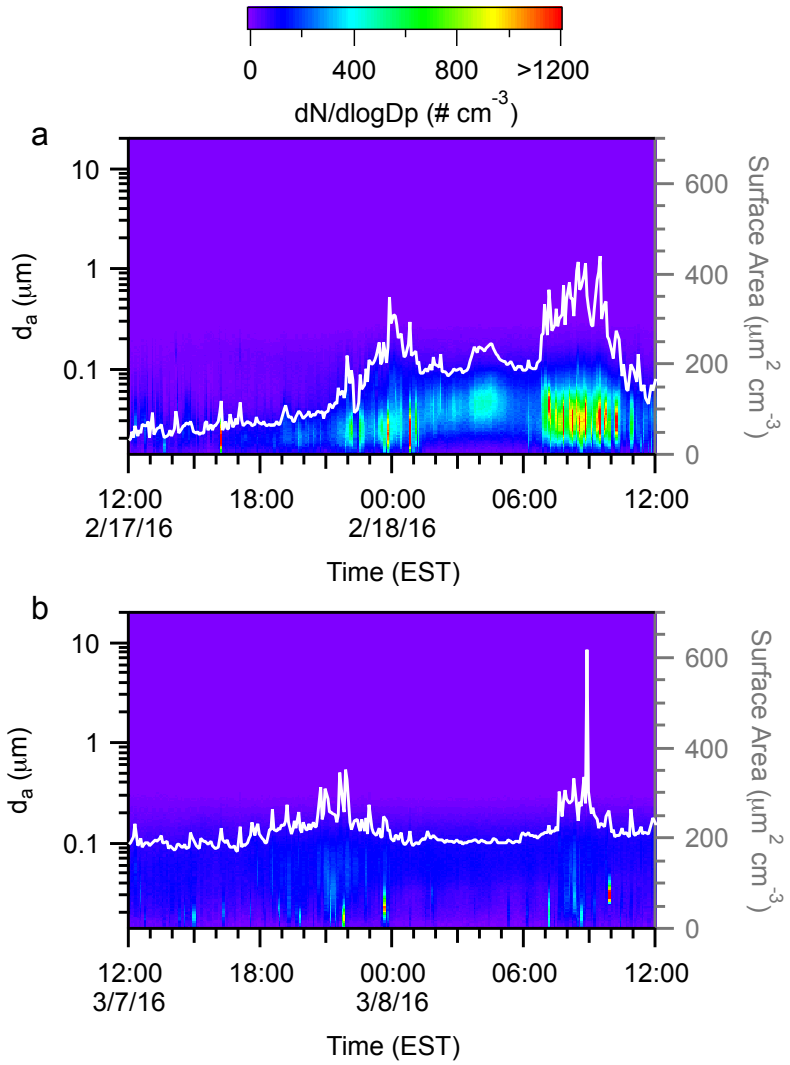

Figure S5 | Size-resolved aerodynamic diameter (d_a) particle number concentrations and total particle surface area concentrations (*white traces*) for the two case study time periods (all times EST): (**a**) 12:00 February 17 – 12:00 February 18, and (**b**) 12:00 March 7 to 12:00 March 8.

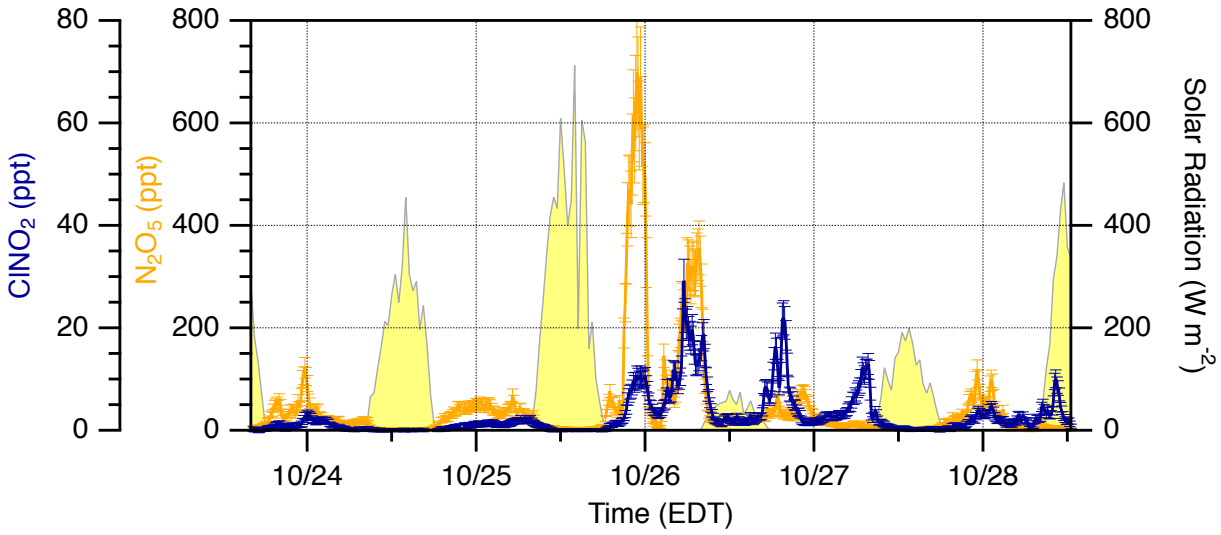

Figure S6 | October 2016 measurements of $ClNO_2$ and N_2O_5 in Ann Arbor, Michigan. 10 min averaged $ClNO_2$ and N_2O_5 mole ratios, as well as solar radiation, from October 23-28, 2016. Error bars represent CIMS measurement uncertainty.

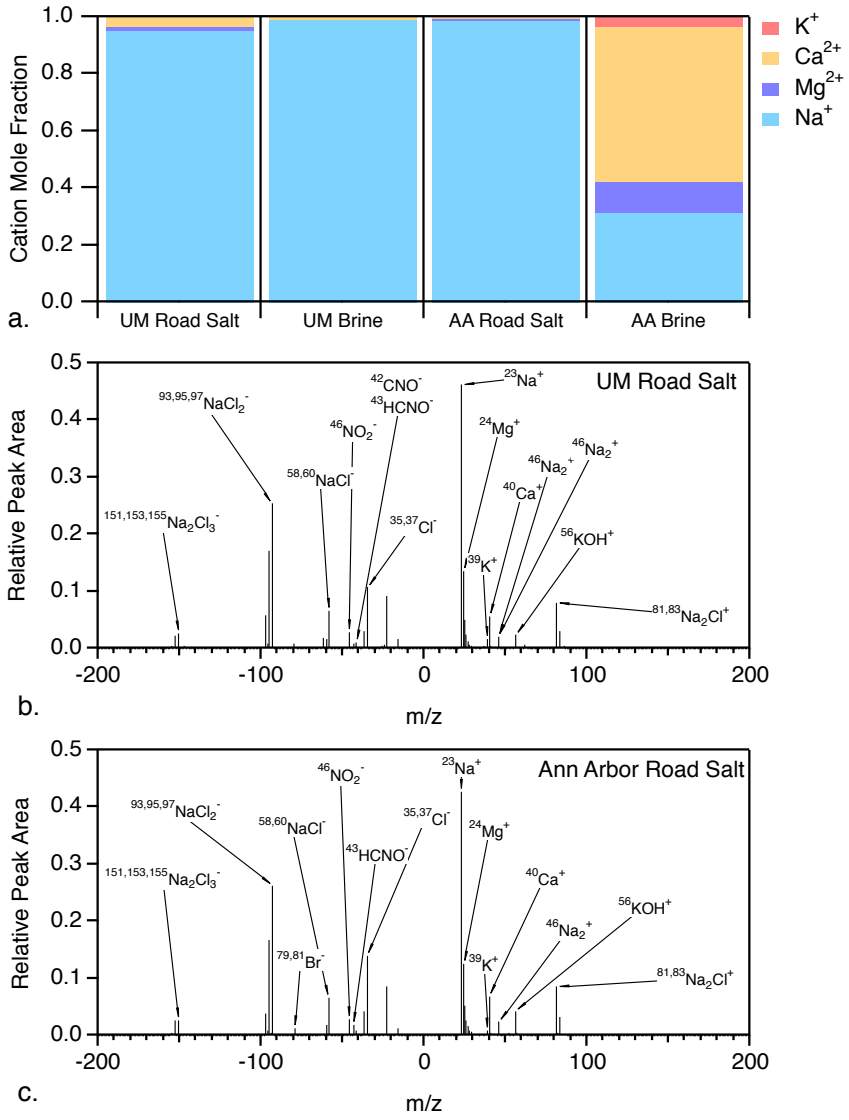

Figure S7 | Characterization of road salts and brine used for deicing. Inorganic cation mole fractions of road salts and brines used by the city of Ann Arbor (AA) and the University of Michigan (UM) campus (**a**). Chloride was the only inorganic anion observed above the IC detection limits. Average ATOFMS individual particle dual-polarity mass spectra of road salt samples from (**b**) city of Ann Arbor and (**c**) the University of Michigan (UM).

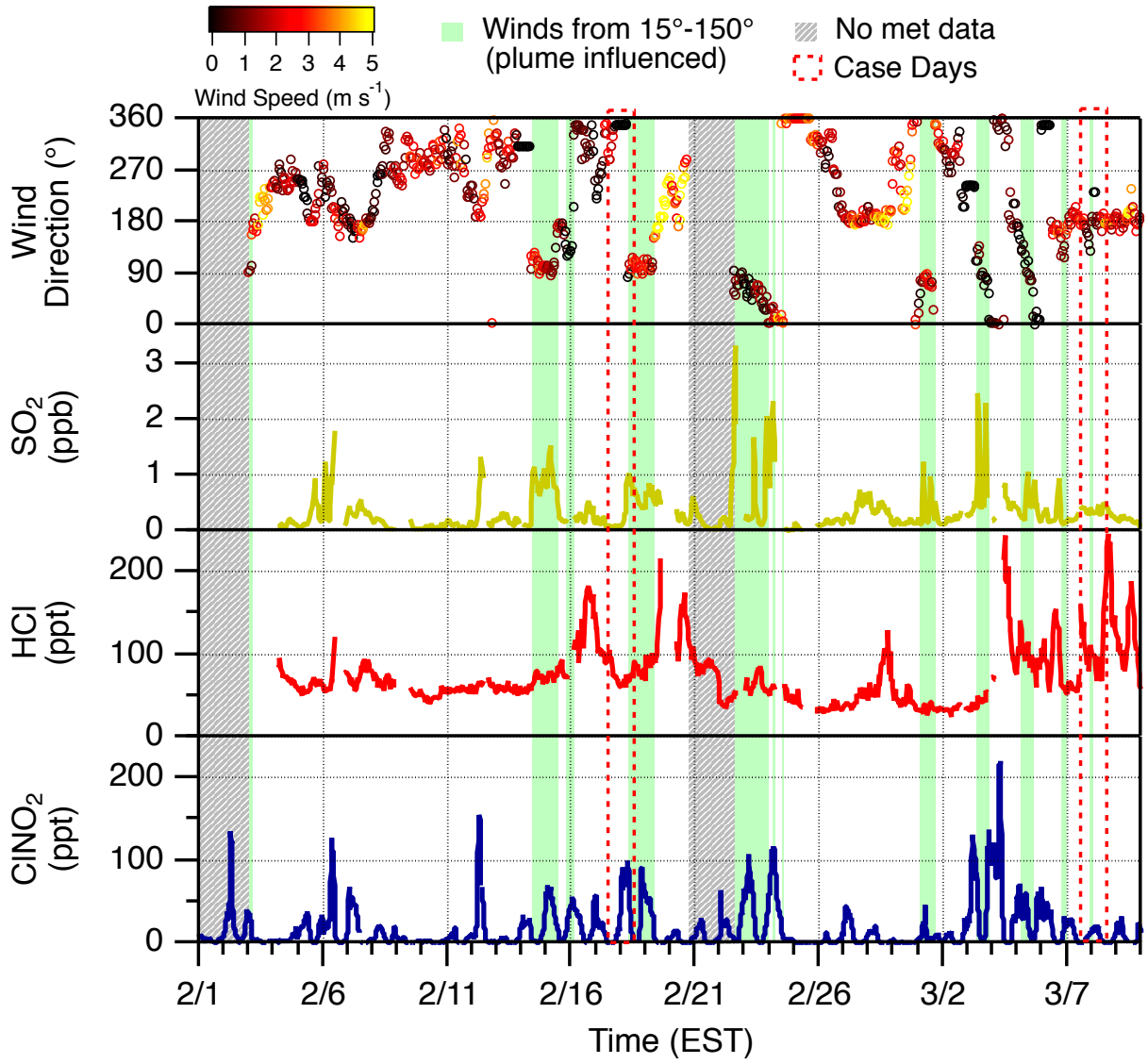

Figure S8 | Identification of potential power plant/industrial plume influence on the sampling site (green shading), when winds (*top panel*, color scale = wind speed) came from the 15° to 150° direction. Hourly AIM-IC measurements of pollution plume tracers, SO_2 and HCl (*middle panels*), and CIMS 10 min averaged $ClNO_2$ measurements (*bottom panel*), from February 1 to March 10, 2016. Gray shading represents periods when wind measurements were unavailable. Dashed red boxes represent the two case study days: February 17-18 and March 7-8, 2016.

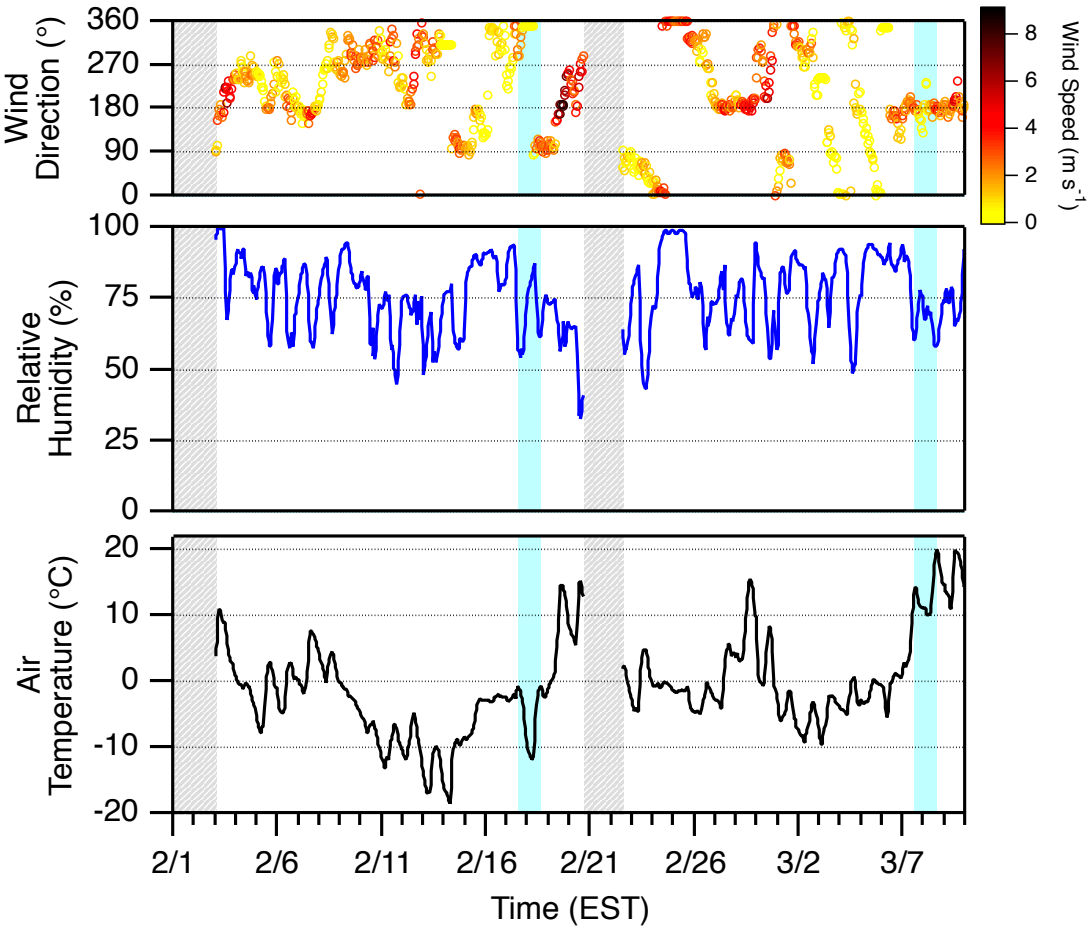

Figure S9 | Meteorological parameters from February 1 to March 10, 2016. Hourly averaged wind speed and direction (*top*), relative humidity (*middle*), and air temperature (*bottom*) from the nearby CWOP weather station. The blue shaded regions represent the two case periods (February 17-18 and March 7-8, 2016), and the gray shading represents periods of no data.

SECTION S4. SUPPLEMENTARY REFERENCES

(1) Thaler, R. D.; Mielke, L. H.; Osthoff, H. D. Quantification of Nitryl Chloride at Part per Trillion Mixing Ratios by Thermal Dissociation Cavity Ring-down Spectroscopy. *Anal. Chem.* **2011**, *83*, 2761–2766. https://doi.org/10.1073/pnas.1201800109.

(2) Sjostedt, S. J.; Huey, L. G.; Tanner, D. J.; Peischl, J.; Chen, G.; Dibb, J. E.; Lefer, B.; Hutterli, M. A.; Beyersdorf, A. J.; Blake, N. J.; et al. Observations of Hydroxyl and the Sum of Peroxy Radicals at Summit, Greenland during Summer 2003. *Atmos. Environ.* **2007**, *41* (24), 5122–5137. https://doi.org/10.1016/j.atmosenv.2006.06.065.

(3) Pollack, I. B.; Lerner, B. M.; Ryerson, T. B. Evaluation of Ultraviolet Light-Emitting Diodes for Detection of Atmospheric NO2by Photolysis - Chemiluminescence. *J. Atmos. Chem.* **2010**, *65* (2–3), 111–125. https://doi.org/10.1007/s10874-011-9184-3.

(4) Bertram, T. H.; Thornton, J. A.; Riedel, T. P.; Middlebrook, A. M.; Bahreini, R.; Bates, T. S.; Quinn, P. K.; Coffman, D. J. Direct Observations of N2O5 Reactivity on Ambient Aerosol Particles. *Geophys. Res. Lett.* **2009**, *36* (October), 1–5. https://doi.org/10.1029/2009GL040248.

(5) Osthoff, H. D.; Roberts, J. M.; Ravishankara, A. R.; Williams, E. J.; Lerner, B. M.; Sommariva, R.; Bates, T. S.; Coffman, D. J.; Quinn, P. K.; Dibb, J. E.; et al. High Levels of Nitryl Chloride in the Polluted Subtropical Marine Boundary Layer. *Nat. Geosci.* **2008**, *1* (5), 324–328. https://doi.org/10.1038/ngeo177.

(6) Markovic, M. Z.; VandenBoer, T. C.; Murphy, J. G. Characterization and Optimization of an Online System for the Simultaneous Measurement of Atmospheric Water-Soluble Constituents in the Gas and Particle Phases. *J. Environ. Monit.* **2012**, *14* (7), 1872. https://doi.org/10.1039/c2em00004k.

(7) Apel, E. C.; UCAR/NCAR. Trace Organic Gas Analyzer (TOGA) for HIAPER https://doi.org/10.5065/D6DF6P9Q (accessed Dec 20, 2016).

(8) Apel, E. C.; Calvert, J. G.; Fehsenfeld, F. C. The Nonmethane Hydrocarbon Intercomparison Experiment Tasks I and 2. *J. Geophys. Res.* **1994**, *99* (D8), 16651–16664.

(9) Apel, E. C.; Calvert, J. G.; Gilpin, T. M.; Fehsenfeld, F. C.; Parrish, D. D.; Lonneman, W. A. The Nonmethane Hydrocarbon Intercomparison Experiment (NOMHICE): Task 3. *J. Geophys. Res. Atmos.* **1999**, *104* (D21), 26069–26086. https://doi.org/10.1029/1999JD900793.

(10) Hornbrook, R. S.; Hills, A. J.; Riemer, D. D.; Abdelhamid, A.; Flocke, F. M.; Hall, S. R.; Huey, L. G.; Knapp, D. J.; Liao, J.; III, R. L. M.; et al. Arctic Springtime Observations of Volatile Organic Compounds during the OASIS-2009 Campaign. *J. Geophys. Res. Atmos.* **2016**, *121*, 9789–9813. https://doi.org/10.1002/2016JD025653.Received.

(11) Wagner, J.; Leith, D. Passive Aerosol Sampler. Part I: Principle of Operation. *Aerosol Sci. Technol.* **2001**, *34* (2), 186–192. https://doi.org/10.1080/027868201300034808.

(12) Moffet, R. C.; Qin, X.; Rebotier, T.; Furutani, H.; Prather, K. A. Chemically Segregated Optical and Microphysical Properties of Ambient Aerosols Measured in a Single-Particle Mass Spectrometer. *J. Geophys. Res. Atmos.* **2008**, *113* (12), 1–11. https://doi.org/10.1029/2007JD009393.

(13) Stull, R. B. *An Introduction to Boundary Layer Meteorology*; Springer Science & Business Media, 2012.

(14) Arya, S. P. S. Parameterizing the Height of the Stable Atmospheric Boundary Layer. *J. Appl. Meteorol.* **1981**, *20*, 1192–1202. https://doi.org/10.1175/1520-

0450(1981)020<1192:pthots>2.0.co;2.
(15) Mielke, L. H.; Furgeson, A.; Odame-ankrah, C. A.; Osthoff, H. D. Ubiquity of ClNO2 in the Urban Boundary Layer of Calgary, Alberta, Canada. *Can. J. Chem.* **2016**, *94*, 1–10.
(16) Riedel, T. P.; Wagner, N. L.; Dubé, W. P.; Middlebrook, A. M.; Young, C. J.; Öztürk, F.; Bahreini, R.; Vandenboer, T. C.; Wolfe, D. E.; Williams, E. J.; et al. Chlorine Activation within Urban or Power Plant Plumes: Vertically Resolved ClNO2 and Cl2 Measurements from a Tall Tower in a Polluted Continental Setting. *J. Geophys. Res. Atmos.* **2013**, *118* (15), 8702–8715. https://doi.org/10.1002/jgrd.50637.
(17) Liu, X.; Qu, H.; Huey, L. G.; Wang, Y.; Sjostedt, S.; Zeng, L.; Lu, K.; Wu, Y.; Hu, M.; Shao, M.; et al. High Levels of Daytime Molecular Chlorine and Nitryl Chloride at a Rural Site on the North China Plain. *Environ. Sci. Technol.* **2017**, No. 2, acs.est.7b03039. https://doi.org/10.1021/acs.est.7b03039.
(18) Lightowlers, P. J.; Cape, J. N. Sources and Fate of Atmospheric HCl in the U.K. and Western Europe. *Atmos. Environ.* **1988**, *22* (1), 7–15. https://doi.org/10.1016/0004-6981(88)90294-6.
(19) Simpson, W. R.; Brown, S. S.; Saiz-Lopez, A.; Thornton, J. A.; Glasow, R. Von. Tropospheric Halogen Chemistry: Sources, Cycling, and Impacts. *Chem. Rev.* **2015**, *115*, 4035–4062. https://doi.org/10.1021/cr5006638.
(20) Toxics Release Inventory (TRI) Program https://www.epa.gov/toxics-release-inventory-tri-program.
(21) Pio, C. A.; Harrison, R. M. The Equilibrium of Ammonium Chloride Aerosol with Gaseous Hydrochloric Acid and Ammonia under Tropospheric Conditions. *Atmos. Environ.* **1987**, *21* (5), 1243–1246. https://doi.org/10.1016/0004-6981(87)90253-8.
(22) Tan, P. V.; Evans, G. J.; Tsai, J.; Owega, S.; Fila, M. S.; Malpica, O.; Brook, J. R. On-Line Analysis of Urban Particulate Matter Focusing on Elevated Wintertime Aerosol Concentrations. *Environ. Sci. Technol.* **2002**, *36* (16), 3512–3518. https://doi.org/10.1021/es011448i.
(23) Allen, A. G.; Harrison, R. M.; Erisman, J. W. Field Measurements of the Dissociation of Ammonium Nitrate and Ammonium Chloride Aerosols. *Atmos. Environ.* **1989**, *23* (7), 1591–1599. https://doi.org/10.1016/0004-6981(89)90418-6.
(24) Wexler, A. S.; Seinfeld, J. H. The Distribution of Ammonium Salts among a Size and Composition Dispersed Aerosol. *Atmos. Environ. Part A, Gen. Top.* **1990**, *24A* (5), 1231–1246. https://doi.org/10.1016/0960-1686(90)90088-5.
(25) Ryder, O. S.; Ault, A. P.; Cahill, J. F.; Guasco, T. L.; Riedel, T. P.; Cuadra-Rodriguez, L. A.; Gaston, C. J.; Fitzgerald, E.; Lee, C.; Prather, K. A.; et al. On the Role of Particle Inorganic Mixing State in the Reactive Uptake of N2O5 to Ambient Aerosol Particles. *Environ. Sci. Technol.* **2014**, *48* (3), 1618–1627. https://doi.org/10.1021/es4042622.
(26) Ahern, A. T.; Goldberger, L.; Jahl, L.; Thornton, J. A.; Sullivan, R. C. Production of N2O5 and ClNO2 through Nocturnal Processing of Biomass-Burning Aerosol. *Environ. Sci. Technol.* **2018**, *52* (2), 550–559. https://doi.org/10.1021/acs.est.7b04386.
(27) Behnke, W.; George, C.; Scheer, V.; Zetzsch, C. Production and Decay of ClNO2 from the Reaction of Gaseous N2O5 with NaCl Solution : Bulk and Aerosol Experiments. *J. Geophys. Res.* **1997**, *102* (D3), 3795–3804. https://doi.org/10.1029/96JD03057.
(28) Bertram, T. H.; Thornton, J. A. Toward a General Parameterization of N2O5 Reactivity on Aqueous Particles: The Competing Effects of Particle Liquid Water, Nitrate and Chloride. *Atmos. Chem. Phys.* **2009**, *9*, 8351–8363.

(29) Chang, W. L.; Bhave, P. V.; Brown, S. S.; Riemer, N.; Stutz, J.; Dabdub, D. Heterogeneous Atmospheric Chemistry, Ambient Measurements, and Model Calculations of N2O5: A Review. *Aerosol Sci. Technol.* **2011**, *45* (6), 665–695. https://doi.org/10.1080/02786826.2010.551672.

(30) Crowley, J. N.; Ammann, M.; Cox, R. A.; Hynes, R. G.; Jenkin, M. E.; Mellouki, A.; Rossi, M. J.; Troe, J.; Wallington, T. J. Evaluated Kinetic and Photochemical Data for Atmospheric Chemistry: Volume v -Heterogeneous Reactions on Solid Substrates. *Atmos. Chem. Phys.* **2010**, *10* (18), 9059–9223. https://doi.org/10.5194/acp-10-9059-2010.

(31) Saathoff, H.; Naumann, K.-H.; Riemer, N.; Kamm, S.; Möhler, O.; Schurath, U.; Vogel, H.; Vogel, B. The Loss of NO2, HNO3, NO3/N2O5, and HO2 /HOONO2 on Soot Aerosol: A Chamber and Modeling Study. *Geophys. Res. Lett.* **2001**, *28* (10), 1957–1960. https://doi.org/10.1029/2000gl012619.